Cell Research (2012) 22:305-320.

www.nature.com/cr

ORIGINAL ARTICLE

The MRE11 GAR motif regulates DNA double-strand break processing and ATR activation

Zhenbao Yu[1], Gillian Vogel[1], Yan Coulombe[2], Danielle Dubeau[1], Elizabeth Spehalski[3], Josée Hébert[4, 5], David O Ferguson[3], Jean Yves Masson[2], Stéphane Richard[1]

[1]Terry Fox Molecular Oncology Group, Bloomfield Center for Research on Aging, Lady Davis Institute for Medical Research, Sir Mortimer B. Davis Jewish General Hospital, and Departments of Oncology and Medicine, McGill University, Montreal, Quebec, Canada H3T 1E2; [2]Genome Stability Laboratory, Laval University Cancer Research Center, Hôtel-Dieu de Québec (CHUQ), Quebec city, Quebec, Canada G1R 2J6; [3]Department of Pathology, University of Michigan Medical School, Ann Arbor, MI 48109, USA; [4]Leukemia Cell Bank of Quebec, and Division of Hematology, Maisonneuve-Rosemont Hospital, Montreal, Quebec, Canada; [5]Department of Medicine, Université de Montréal, Montreal, Quebec, Canada H1T 2M4

The MRE11/RAD50/NBS1 complex is the primary sensor rapidly recruited to DNA double-strand breaks (DSBs). MRE11 is known to be arginine methylated by PRMT1 within its glycine-arginine-rich (GAR) motif. In this study, we report a mouse knock-in allele of *Mre11* that substitutes the arginines with lysines in the GAR motif and generates the MRE11^{RK} protein devoid of methylated arginines. The *Mre11*$^{RK/RK}$ mice were hypersensitive to γ-irradiation (IR) and the cells from these mice displayed cell cycle checkpoint defects and chromosome instability. Moreover, the *Mre11*$^{RK/RK}$ MEFs exhibited ATR/CHK1 signaling defects and impairment in the recruitment of RPA and RAD51 to the damaged sites. The M^{RK}RN complex formed and localized to the sites of DNA damage and normally activated the ATM pathway in response to IR. The M^{RK}RN complex exhibited exonuclease and DNA-binding defects *in vitro* responsible for the impaired DNA end resection and ATR activation observed *in vivo* in response to IR. Our findings provide genetic evidence for the critical role of the MRE11 GAR motif in DSB repair, and demonstrate a mechanistic link between post-translational modifications at the MRE11 GAR motif and DSB processing, as well as the ATR/CHK1 checkpoint signaling.

***Keywords*:** DNA damage signaling; arginine methylation; GAR motif; MRE11; ATR

Cell Research (2012) **22**:305-320. doi:10.1038/cr.2011.128; published online 9 August 2011

Introduction

Protein arginine methylation results in the addition of one or two methyl groups to the guanidino nitrogen atoms of arginine [1]. There are three main forms of methylated arginine identified in eukaryotes: ω-N^G-monomethylarginines, ω-N'^G,N^G-asymmetric dimethylarginines and ω-N^G,N^G-symmetric dimethylarginines. There are nine protein arginine *N*-methylation enzymes (PRMTs) that catalyze the transfer of a methyl group from *S*-adenosylmethionine to a guanidino nitrogen of arginine [2]. Arginines located within glycine-arginine-rich (GAR) motifs are preferred sites of methylation of several PRMTs including PRMT1 [2], the predominant enzyme in mammalian cells, responsible for most of the asymmetrical arginine dimethylation reactions in human cells [3]. *PRMT1*-null mice are embryonically lethal and contain numerous hypomethylated substrates [4]. Using a conditional null *PRMT1* allele in mice, it was shown that *PRMT1*-deficient mouse embryonic fibroblasts (MEFs) exhibit spontaneous DNA damage, chromosome instability, polyploidy and defective checkpoint activation following DNA damage [5]. These findings highlight the importance of arginine methylation in the DNA damage response pathway and the maintenance of genomic stability. A large number of GAR motif-containing proteins were shown to be arginine methylated using candidate and proteomic approaches [6]. These substrates are func-

Correspondence: Stéphane Richard
Tel: 514 340 8260; Fax: 514 340 8295
E-mail: stephane.richard@mcgill.ca
Received 30 March 2011; revised 26 May 2011; accepted 7 Jun 2011; published online 9 August 2011

tionally involved in diverse intracellular processes from nuclear export and gene expression to DNA damage signaling [2].

The MRE11/Rad50/NBS1 (MRN) complex is the primary sensor rapidly recruited to DNA double-strand breaks (DSBs) [7-9]. The MRN complex tethers the DNA ends [10, 11], leading to the recruitment and activation of the ATM kinase [12, 13]. The MRN complex is also thought to participate in ATR-CHK1 kinase activation by facilitating DNA end resection [14-18]. It participates in multiple downstream pathways for checkpoint signaling, DNA replication, telomere maintenance, non-homologous end joining and meiotic recombination [19-24].

The *in vivo* function of the MRN complex has been revealed by hypomorphic alleles in human *MRE11* and *NBS1*, leading to ataxia-telangiectasia-like disorder (ATLD) and Nijmegen breakage syndrome (NBS), respectively [25, 26]. These disorders share characteristic features including hypersensitivity to ionizing radiation, immunodeficiency and an increased predisposition to the development of malignancies [27]. The *in vivo* deletion of components of the MRN complex is embryonically lethal in mice [28-31]. However, animal models of ATLD ($Mre11^{ATLD1/ATLD1}$) and NBS have been generated and share many common features of the human disorders [32, 33].

MRE11 is a conserved protein with an N-terminal nuclease domain [11, 34] and a DNA-binding region [10, 35] encompassing the GAR motif [36]. MRE11 nuclease-defective mice have been generated ($Mre11^{H129N/H129N}$), defining a physiological role of the MRE11 nuclease activity in homologous recombination and the maintenance of genomic stability [30]. Mammalian MRE11 is also involved in the classical and alternative non-homologous end-joining (NHEJ) pathways [21, 23]. The arginines within the MRE11 GAR motif are asymmetrically dimethylated by PRMT1 and have been shown to regulate its exonuclease activity *in vitro* [36, 37], but the physiological significance of arginine methylation remains to be elucidated. In this study, we generated an *Mre11* allele ($Mre11^{RK}$) in mice that substitutes the arginines with lysines within the GAR motif. We report the requirement for the MRE11 GAR motif in regulating the ATR activation during DNA damage signaling and the maintenance of genomic stability.

Results

Generation of $Mre11^{RK}$ knock-in mice

We generated a mouse knock-in allele at the *Mre11* locus that substitutes the nine arginines within the GAR motif with lysines (Figure 1A). This $Mre11^{RK}$ allele was generated to assess the *in vivo* physiological role of the methylarginines within the MRE11 GAR motif. Lysine was chosen to maintain the positive charge of the residues. The $Mre11^{RK}$ allele was generated by homologous recombination targeting exon 14 that encodes the GAR motif (Figure 1B). Mouse genotypes were verified by PCR using genomic DNA (Figure 1C). Moreover, the genomic DNA and the mRNA expressed from this mutant allele were sequenced, verifying that the codons encoding the nine arginines within the GAR motif were replaced with lysine-encoding codons (data not shown). The $Mre11^{RK}$ allele was also engineered to introduce an *Eco*RI site within the middle of the exon 14 to distinguish the mRNAs encoding wild-type *Mre11* and $Mre11^{RK}$. As expected, the DNA fragment generated by RT-PCR spanning the exon 14 was undigested by *Eco*RI in wild-type cells, digested 50% and 100% in $Mre11^{RK/+}$ and $Mre11^{RK/RK}$ cells, respectively, further confirming the genotypes (Figure 1D).

The $Mre11^{RK/RK}$ mice were born in the expected Mendelian ratio and did not display any overt phenotypes (data not shown), unlike the $Mre11^{\Delta/\Delta}$ and $Mre11^{H129N/H129N}$ nuclease-defective mice, which die during early embryogenesis [30]. The $Mre11^{RK/RK}$ females and males were fertile and gave rise to normal litter sizes of six to eight pups (data not shown), unlike the $Mre11^{ATLD1/ATLD1}$ mice where the females are subfertile [32].

$Mre11^{RK/RK}$ mice and MEFs are hypersensitive to γ-IR

We first decided to challenge the mice with γ-irradiation (IR), as a known phenotype of MRN hypomorphic alleles is their hypersensitivity to IR. Cohorts of $Mre11^{+/+}$, $Mre11^{RK/+}$ and $Mre11^{RK/RK}$ mice were irradiated with 10 Gy of IR and closely monitored for radiation toxicity. All of the $Mre11^{RK/RK}$ mice succumbed to 10 Gy of IR treatment within ~2 weeks, while less than half of the wild-type and the $Mre11^{RK/+}$ mice died within 35 days (Figure 2A).

The hypersensitivity to IR was also demonstrated in the cells isolated from $Mre11^{RK/RK}$ mice. Immortalized $Mre11^{RK/RK}$ and wild-type MEFs were generated and treated with varying IR doses. After IR treatment, the cell colony number was significantly reduced in $Mre11^{RK/RK}$ MEFs, demonstrating more than 100-fold hypersensitivity to IR compared to wild-type MEFs (Figure 2B).

MRE11 participates in NHEJ pathways [21, 23], which are required for class switch recombination (CSR). Complete absence of MRE11 in developing B lymphocytes causes a significant reduction in CSR, whereas MRE11 defective only in nuclease activities causes a mild CSR defect [23]. To determine if the MRE11 GAR

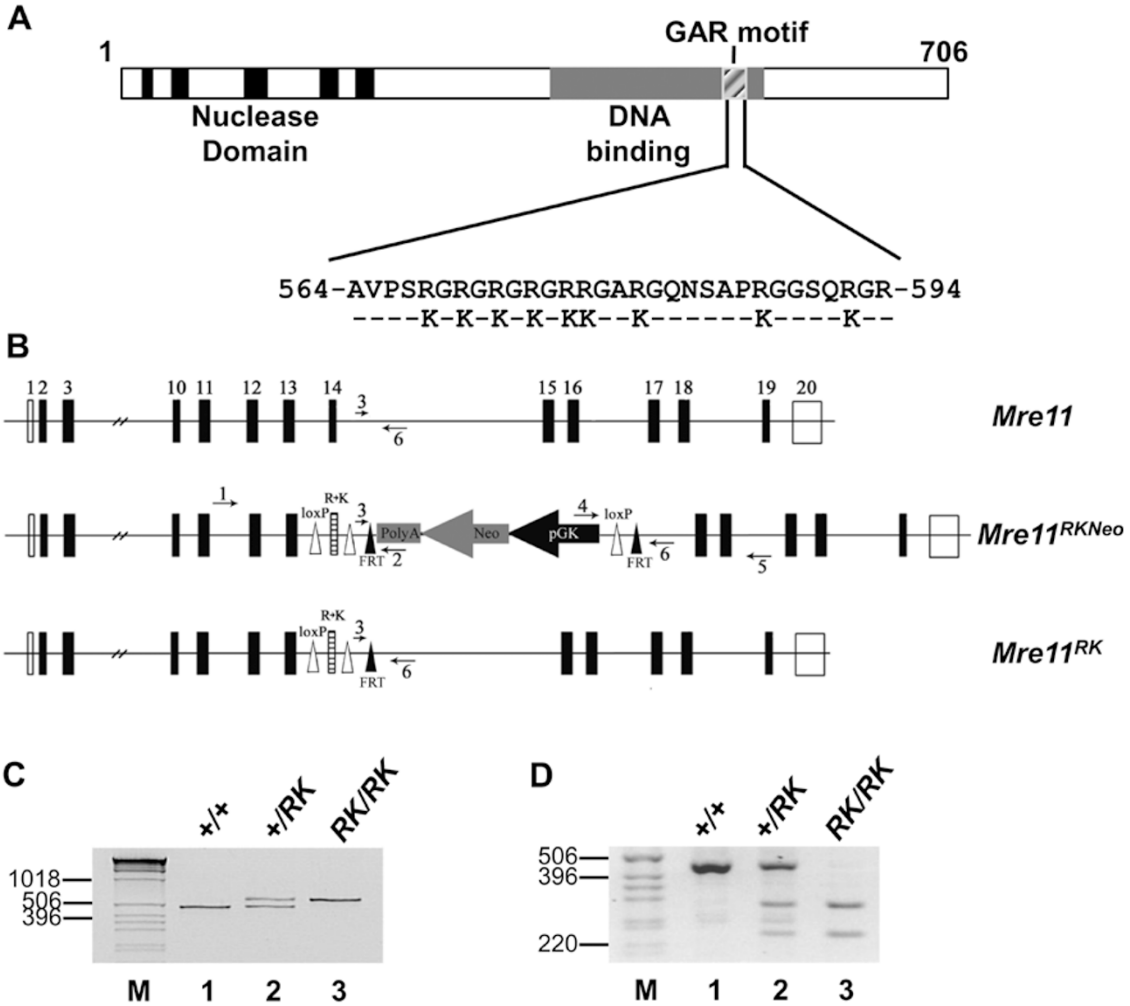

Figure 1 Generation of *Mre11*$^{RK/RK}$ mice and MEF cells. **(A)** Schematic representation of the wild-type MRE11 with the glycine-arginine rich (GAR) motif and the sequence of MRE11^{RK} substituting the arginine with lysine residues. **(B)** Schematic representation of the mouse *Mre11* allele and *Mre11*^{RK} allele. The initial strategy (*MRE11*^{RKNeo}) shows the targeting position at the exon 14, with substitution of arginine with lysine residues as shown in **A** and the targeting plasmid structural elements. Shown in *Mre11*^{RK} is the targeted locus with deletion of Neo. The exons are the black boxes and the line represents introns not drawn to scale. The white and blank triangles denote loxP sites and FRT sites, respectively, and the small arrows denote the primers used for PCR analysis. The expected size of the PCR DNA fragment amplified by the primer pair of primer 3 and primer 6 for the wild-type allele is 525 bp, while the size of the DNA fragment for the *Mre11*^{RK} allele is 591 bp. **(C)** Genomic DNA isolated from primary MEFs was analyzed by PCR using the primer pair of primer 3 and primer 6 as indicated in **B** and the DNA fragments visualized on an ethidium-bromide-stained agarose gel. M denotes molecular mass markers of the 1 kb ladder (Invitrogen). **(D)** Total cellular RNA was isolated from primary MEFs and subjected to reverse transcription-PCR. The DNA fragment was purified and digested with *Eco*RI and then separated on an agarose gel. M denotes molecular mass markers of the 1 kb ladder (Invitrogen).

motif is required for its function in NHEJ, we compared the impact on CSR of *Mre11*$^{RK/RK}$ to that of *Mre11*$^{\Delta/\Delta}$ and *Mre11*$^{\Delta/H129N}$. Conversion of *Mre11*^{cond} to *Mre11*$^{\Delta}$ in mature IgM+ B lymphocytes was facilitated by the CD21-Cre transgene [23, 38]. CSR was assessed in B lymphocytes isolated from spleens. Comparing *Mre11*$^{RK/RK}$ to *Mre11*$^{+/+}$, no difference in spleen size or cellularity was evident (data not shown). We induced switching from IgM to IgG1 and noted defects in *Mre11*$^{\Delta/\Delta}$ and *Mre11*$^{\Delta/H129N}$ cells similar to those reported previously (Figure 2C, 2D) [23]. In contrast, *Mre11*$^{RK/RK}$ cells display a small statistically significant difference (P = 0.0409), which is unlikely to be biologically significant (Figure 2C, 2D). Taken together, these findings show that we have gener-

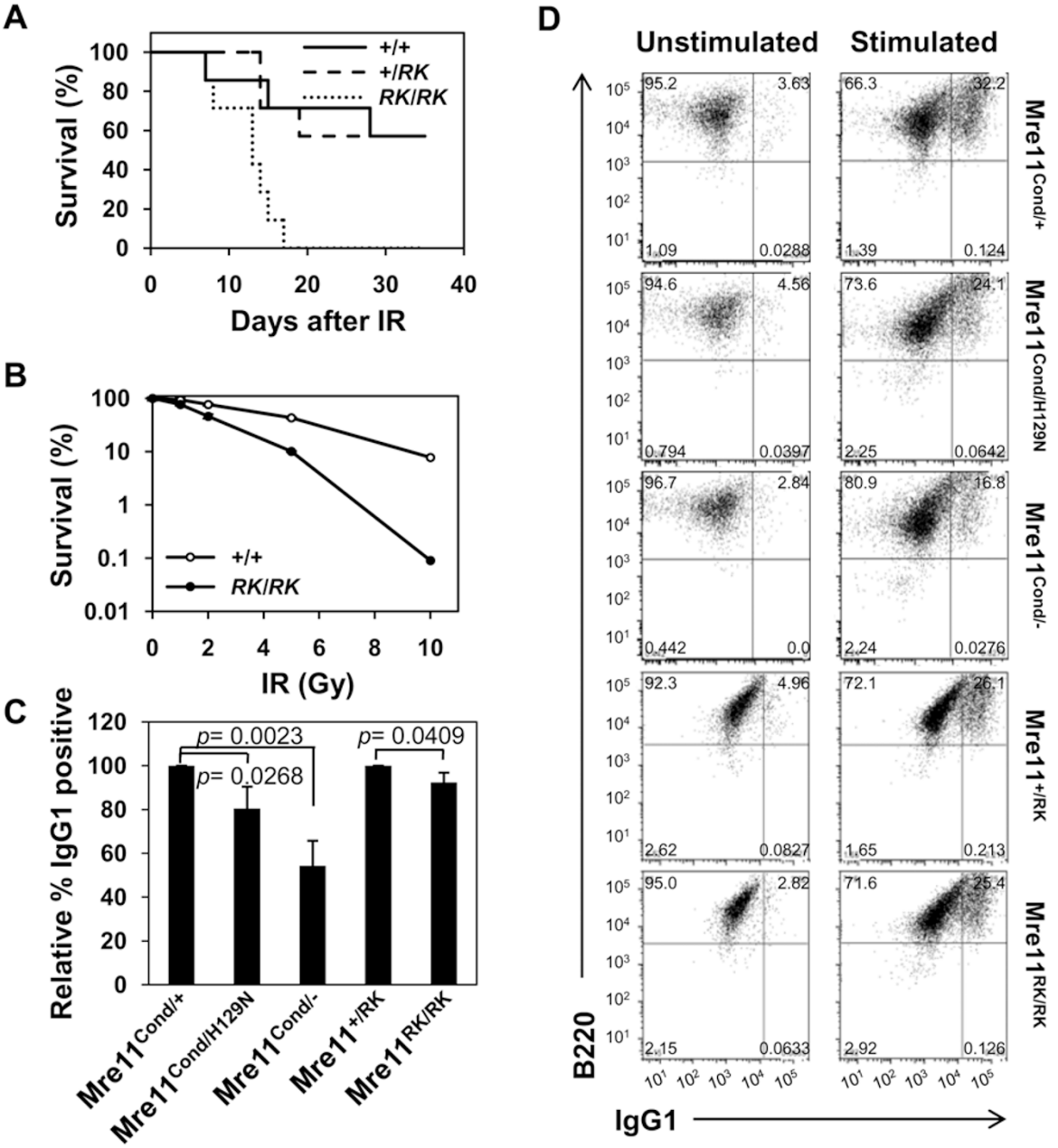

Figure 2 *Mre11*$^{RK/RK}$ mice and MEFs are hypersensitive to IR, but the B lymphocytes have no significant impact on class switching recombination. **(A)** *Mre11*$^{+/+}$, *Mre11*$^{+/RK}$ and *Mre11*$^{RK/RK}$ mice were treated with 10 Gy IR and monitored for signs of radiation toxicity over 35 days. *Mre11*$^{RK/RK}$ mice showed a significant reduction in survival rates compared to *Mre11*$^{+/+}$ and *Mre11*$^{+/RK}$ mice according to the log-rank test (P = 0.0066). The percentage survival was plotted as a function of days post IR. **(B)** Approximately 200-400 immortalized MEFs were seeded on a 10 cm tissue culture dish and treated with various doses of IR. The cells were then maintained in regular medium. Fourteen to twenty days later, the cells were fixed and cell colonies were stained with crystal violet and counted. The colony number was normalized to percentage of untreated cells and plotted as a function of IR dosage. The graphs shown represent the average and standard deviation (SD) from four independent immortalized MEF cell lines (clones) of each genotype. The asterisks denotes $P < 0.01$ using the Student's *t*-test. **(C)** Flow cytometric analysis of immunoglobulin class switching from IgM to IgG in B lymphocytes cultured with IL-4 and anti-CD40 for four days. Bar graph depicts comparisons of IgG1+ cell populations relative to *Mre11*$^{+/cond}$ control, from an average (+SD) of three mice per genotype. *Mre11*^{cond} is *Mre11*$^{\Delta}$ in B lymphocytes. **(D)** Flow cytometric analysis of immunoglobulin class switching from IgM to IgG in B lymphocytes cultured with IL-4 and anti-CD40 for 4 days shown in panel **C**.

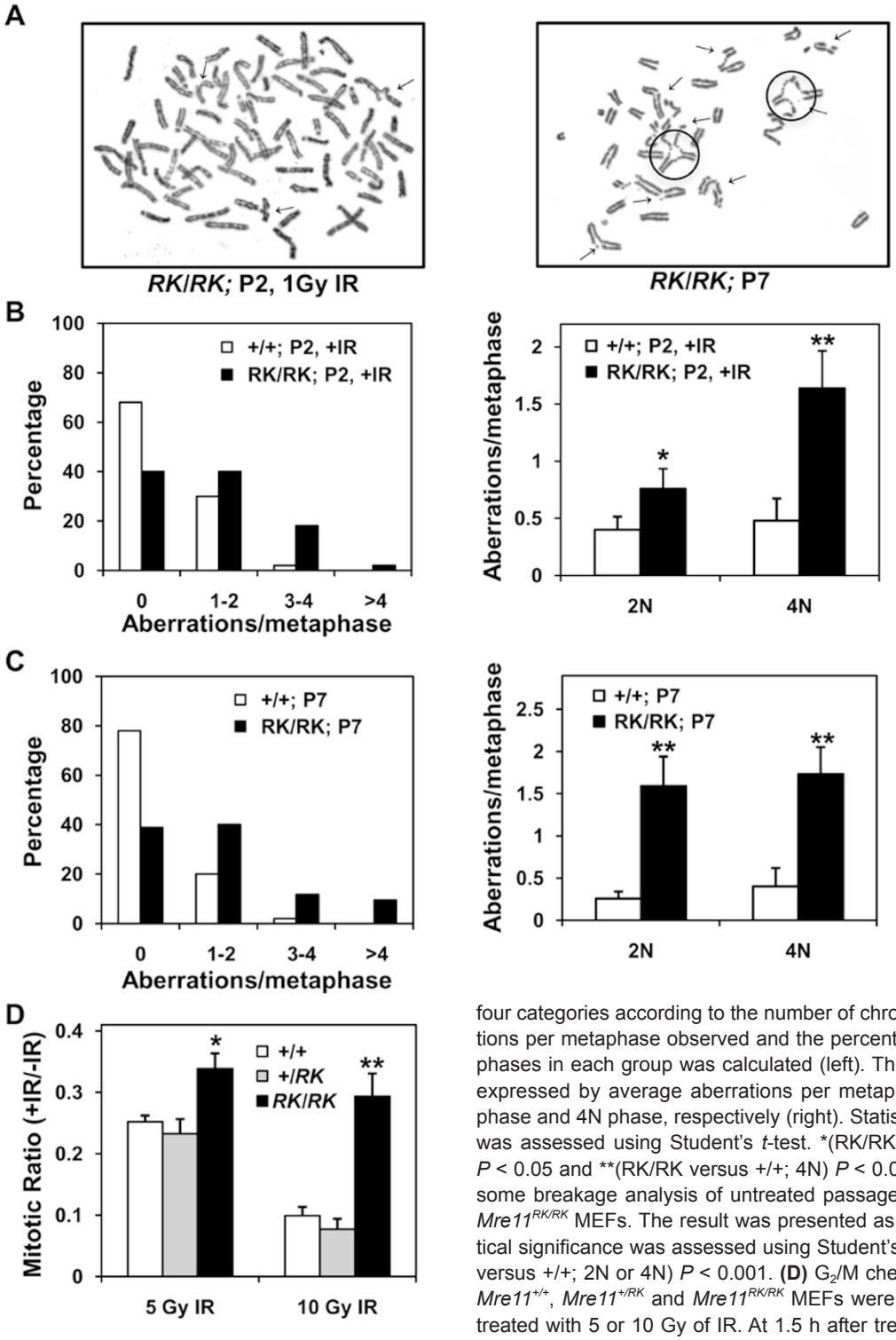

Figure 3 Chromosomal instability and DNA damage checkpoint defect in *Mre11*$^{RK/RK}$ MEFs. **(A)** Representative metaphases from IR-treated passage 2 *Mre11*$^{RK/RK}$ MEF cells (left) and untreated passage 7 *Mre11*$^{RK/RK}$ MEF cells (right). Breaks were indicated by arrows and radial chromosomes were cycled. **(B)** Chromosome breakage analysis of IR-treated passage 2 wild-type and *Mre11*$^{RK/RK}$ MEFs. The metaphases were grouped into four categories according to the number of chromosome aberrations per metaphase observed and the percentage of the metaphases in each group was calculated (left). The data were also expressed by average aberrations per metaphase at both 2N phase and 4N phase, respectively (right). Statistical significance was assessed using Student's *t*-test. *(RK/RK versus +/+; 2N) $P < 0.05$ and **(RK/RK versus +/+; 4N) $P < 0.001$. **(C)** Chromosome breakage analysis of untreated passage 7 wild-type and *Mre11*$^{RK/RK}$ MEFs. The result was presented as that in **B**. Statistical significance was assessed using Student's *t*-test. **(RK/RK versus +/+; 2N or 4N) $P < 0.001$. **(D)** G_2/M checkpoint analysis. *Mre11*$^{+/+}$, *Mre11*$^{+/RK}$ and *Mre11*$^{RK/RK}$ MEFs were left untreated or treated with 5 or 10 Gy of IR. At 1.5 h after treatment, the cells were fixed and stained with propidium iodide and anti-pS10-histone H3 antibody to identify the cells in mitosis. The percentage of pS10-histone H3-positive cells was determined by flow cytometry and expressed as a ratio of IR treated to non-IR treated. The experiments were performed more than three times for each dosage. Statistical significance was assessed using Student's *t*-test. *(RK/RK versus +/+ or +/RK; 5 Gy) $P < 0.01$ and **(RK/RK versus +/+ or +/RK; 10 Gy) $P < 0.001$.

Table 1 *Mre11*$^{RK/RK}$ MEFs accumulate radial chromosomes

Sample ID	Number of cells	Number of radial figures
WT/WT, passage 2, + 1Gy IR	50	0
RK/RK, passage 2, + 1Gy IR	50	1
WT/WT, passage 7, no IR	50	0
RK/RK, passage 7, no IR	85	11

ated a novel *Mre11* hypomorphic allele and that the GAR motif affects sensitivity to IR, but has no major effects on mouse viability, fertility or CSR.

Defective genomic stability and checkpoint control in Mre11$^{RK/RK}$ *MEFs*

Metaphase spreads were then prepared to determine chromosome damage with passage 2 primary *Mre11*$^{RK/RK}$ and wild-type MEFs treated with 1 Gy of IR. We observed a significant increase in chromosomal anomalies in these *Mre11*$^{RK/RK}$ MEFs (Figure 3A, left panel, and quantified in Figure 3B). Genomic instability was also observed in later stage *Mre11*$^{RK/RK}$ MEFs without DNA damage treatment (Figure 3A, right panel, and quantified in Figure 3C). For example, in passage 7 primary cells, ~60% of *Mre11*$^{RK/RK}$ MEFs harbored at least one chromosome aberration per metaphase, compared to 22% in wild-type cells (Figure 3C). Interestingly, we observed a significant number of radial chromosomes in the passage 7 *Mre11*$^{RK/RK}$ MEFs but not in the wild-type MEFs (Figure 3A, right panel and Table 1). These findings demonstrate the requirement for the MRE11 GAR motif for the maintenance of chromosomal stability.

In response to DNA damage, cell cycle checkpoints are activated to arrest cell cycle progression, allowing time for repair [39]. ATLD cells are known to have checkpoint defects in response to DNA damage [25, 32]. To examine the activation of the G_2/M checkpoint of *Mre11*$^{RK/RK}$ MEFs, we measured the abundance of cells entering mitosis 90 min after IR treatment with anti-histone H3pS10 antibody and expressed it as a mitotic ratio with untreated cells. After 10 Gy IR treatment, a mitotic ratio of ~0.1 was observed for wild-type and *Mre11*$^{+/RK}$ MEFs, suggesting that ~10% of the cells progressed through M phase (Figure 3D). By contrast, a mitotic ratio of ~0.3 was observed for *Mre11*$^{RK/RK}$ MEFs, suggesting that ~30% of the cells progressed through the M phase (Figure 3D). A similar significant difference was also observed with 5 Gy IR (Figure 3D), suggesting that a significant fraction of the *Mre11*$^{RK/RK}$ cells lost their G_2/M checkpoint.

MRN complex formation, localization to sites of DNA damage and ATM activation are normal in Mre11$^{RK/RK}$ *MEFs*

To define the molecular defects observed in *Mre11*$^{RK/RK}$ cells, we first assessed the integrity of the M^{RK}RN complex. Using control and MRE11 immunoprecipitations, we showed that the MRE11^{RK} protein was slightly less

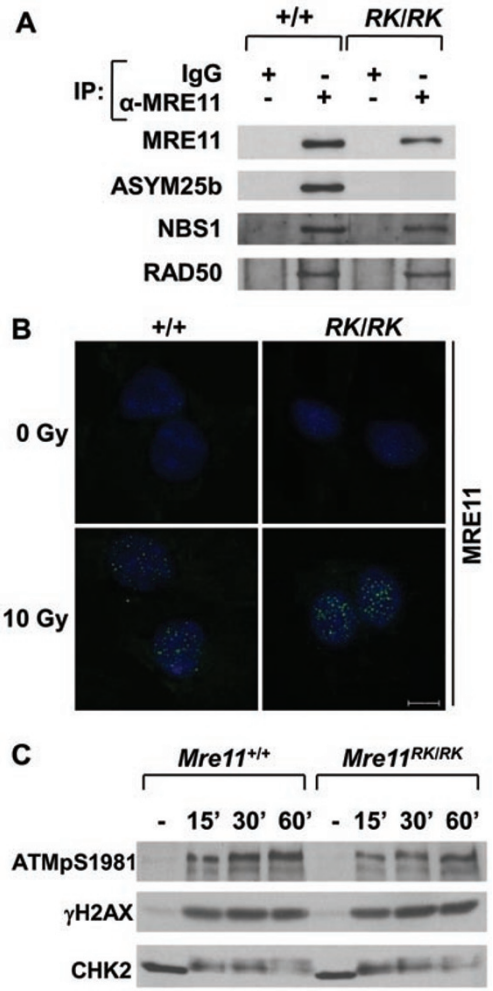

Figure 4 MRN complex formation, localization to sites of DNA damage and IR-induced ATM activation are normal in *Mre11*$^{RK/RK}$ MEFs. **(A)** Whole-cell lysates from wild-type and *Mre11*$^{RK/RK}$ MEFs, respectively, were immunoprecipitated with anti-MRE11 antibody. The bound proteins were separated by SDS-PAGE and immunoblotted with indicated antibodies. **(B)** *Mre11*$^{+/+}$ and *Mre11*$^{RK/RK}$ MEFs were treated with 10 Gy of IR or left untreated. Two hours later, the cells were visualized by indirect immunofluorescence with anti-MRE11 antibody. The scale bar represents 10 μm. **(C)** *Mre11*$^{+/+}$ and *Mre11*$^{RK/RK}$ MEFs were treated with 10 Gy of IR or left untreated (−). The cells were harvested at the indicated times after IR treatment. Total cellular proteins were subjected to immunoblotting with anti-ATMpS1981, anti-γH2AX and anti-CHK2 antibodies.

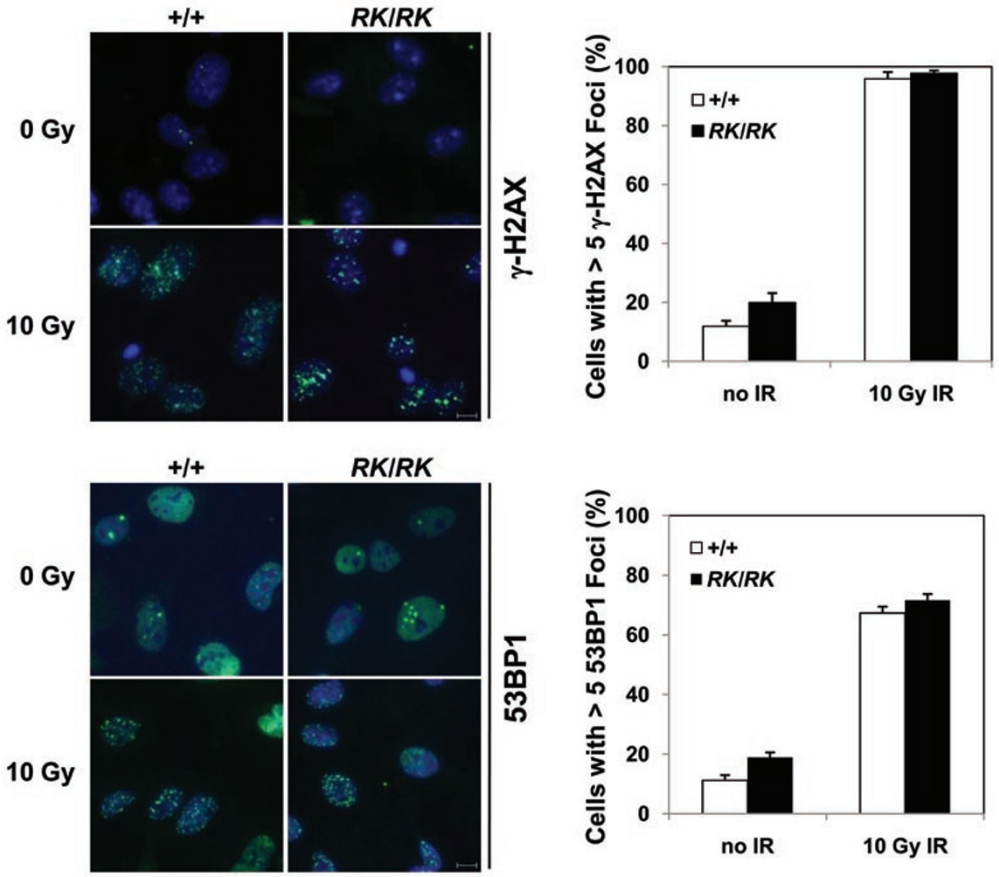

Figure 5 IR-induced nuclear foci of γH2AX and 53BP1 are normal in *Mre11*$^{RK/RK}$ MEFs. Wild-type (*Mre11*$^{+/+}$) and *Mre11*$^{RK/RK}$ MEF cells, respectively, were left untreated or treated with 10 Gy of IR. After 2 h of recovery, the cells were visualized by indirect immunofluorescence with anti-γH2AX and anti-53BP1 antibodies, respectively. Cells with > 5 foci were counted and expressed as a percentage. The graphs show the average and standard error of the mean from two independent experiments performed in duplicates, where > 20 different fields were analyzed. In total more than 500 cells were counted for each sample in each experiment. The scale bar represents 10 μm.

abundant than endogenous MRE11, but it maintained its interaction with NBS1 and RAD50 (Figure 4A). We also investigated the arginine methylation status of MRE11^{RK} with the anti-methylarginine-specific antibody ASYM25b. Indeed, MRE11^{RK} was hypomethylated in *Mre11*$^{RK/RK}$ MEFs (Figure 4A), and the newly introduced lysines were not acetylated (Supplementary information, Figure S1). We next examined the ability of the M^{RK}RN complex to localize to sites of DNA damage by indirect immunofluorescence. MRE11^{RK} localized at sites of DNA damage in response to IR treatment similar to wild-type MRE11 (Figure 4B). These findings show that MRE11^{RK} maintains interactions within the MRN complex.

We next examined whether *Mre11*$^{RK/RK}$ MEFs harbor defects in ATM activation, since MRE11 is required for recruiting and activating the kinase and cells with MRE11 deficiencies are impaired in this pathway [12, 25, 30, 32]. The dynamic of ATM activation was normal in *Mre11*$^{RK/RK}$ MEFs following IR, as assessed by ATM autophosphorylation using the anti-ATMpS1981 antibody [40] and by evaluating phosphorylation of the ATM substrate CHK2, visualized as a slower migrating species by SDS-PAGE (Figure 4C). Moreover, the IR-induced foci of γ-H2AX and 53BP1 were equally formed in *Mre11*$^{RK/RK}$ and the wild-type MEFs (Figure 5), consistent with the M^{RK}RN complex properly localizing at DSBs, resulting in ATM activation.

Defective CHK1 activation in Mre11$^{RK/RK}$ *MEFs in response to IR treatment*

Cells from ATLD patients have both impaired ATM activation and G_2/M checkpoint control [32], whereas the MRE11 nuclease-defective cells have both normal ATM activation and G_2/M checkpoint control, although

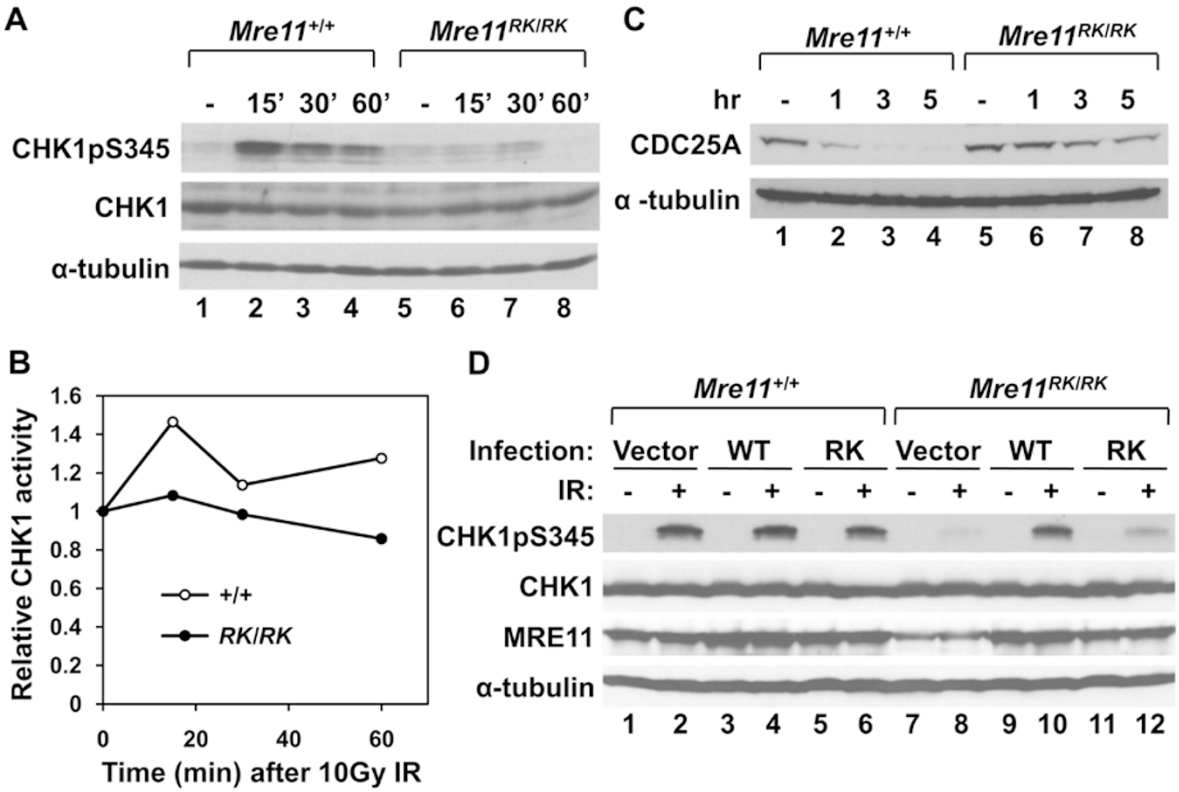

Figure 6 IR-induced CHK1 phosphorylation and activation are defective in *Mre11*$^{RK/RK}$ MEFs. **(A)** *Mre11*$^{+/+}$ and *Mre11*$^{RK/RK}$ MEFs were treated with 10 Gy of IR or left untreated (−). The cells were harvested at the indicated times after IR treatment. Total cellular proteins were subjected to immunoblotting with the indicated antibodies. **(B)** *Mre11*$^{+/+}$ and *Mre11*$^{RK/RK}$ MEFs were treated with 10 Gy of IR or left untreated (−). The cells were harvested at the indicated times after IR treatment, and whole-cell lysates were subjected to immunoprecipitation with the anti-CHK1 antibody. The bound proteins were used for CHK1 activity assay as described in Materials and Methods. **(C)** MEFs were treated as in **A**. The cells were harvested at the indicated times after IR treatment. Total cellular proteins were subjected to immunoblotting with the anti-CDC25A and anti-α-tubulin antibodies as a loading control. **(D)** MEFs were infected with the empty retroviral vector pMSCV-puro (Vector) or the vector which expresses wild-type human MRE11 (WT) or MRE11 RK mutant (RK). The infected cells were selected with 2 μg/ml of puromycin for 2 days after infection. The cells were then treated with 10 Gy of IR (+) or left untreated (−). The cells were harvested at 15 min after IR treatment. Total cellular proteins were subjected to immunoblotting with the indicated antibodies.

MRE11 nuclease activity is essential for cell survival and DNA damage repair [30]. Therefore, the *Mre11*^{RK} hypomorphic allele provides a unique genetic system to assay ATM-independent MRE11 contributions to G_2/M checkpoint control in mammalian cells. It has been proposed that the dual action of ATM and ATR is required to initiate the G_2/M checkpoint in response to IR [41]. Moreover, ATM and MRE11 are required to enhance IR-induced ATR-dependent CHK1 phosphorylation [14, 42], but the role of MRE11 and its GAR motif in ATR activation remains unclear. To assess ATR function, we monitored the phosphorylation of CHK1 using anti-CHK1pS345 antibodies. We observed a dramatic defect in CHK1 activation in *Mre11*$^{RK/RK}$ MEFs compared to wild-type cells in response to IR treatment (Figure 6A). A CHK1 activation defect was also observed in *Mre11*$^{RK/RK}$ MEFs by immunoprecipitating CHK1 and assaying its activity using an *in vitro* kinase assay (Figure 6B). CDC25A is a CHK1 substrate and its phosphorylation is required for its ubiquitination and degradation in response to IR [43]. We observed that CDC25A degradation was impaired in *Mre11*$^{RK/RK}$ MEFs, compared to wild-type MEFs, after IR treatment, consistent with the *Mre11*$^{RK/RK}$ MEFs exhibiting a CHK1 activation defect (Figure 6C). We also observed a mild defect in CHK1 phosphorylation in *Mre11*$^{RK/RK}$ MEFs compared to wild-type cells in response to UV and hydroxyurea treatment, respectively (Supplementary information, Figure S2).

We next performed a rescue experiment with ectopic expression of wild-type MRE11 and MRE11^{RK}

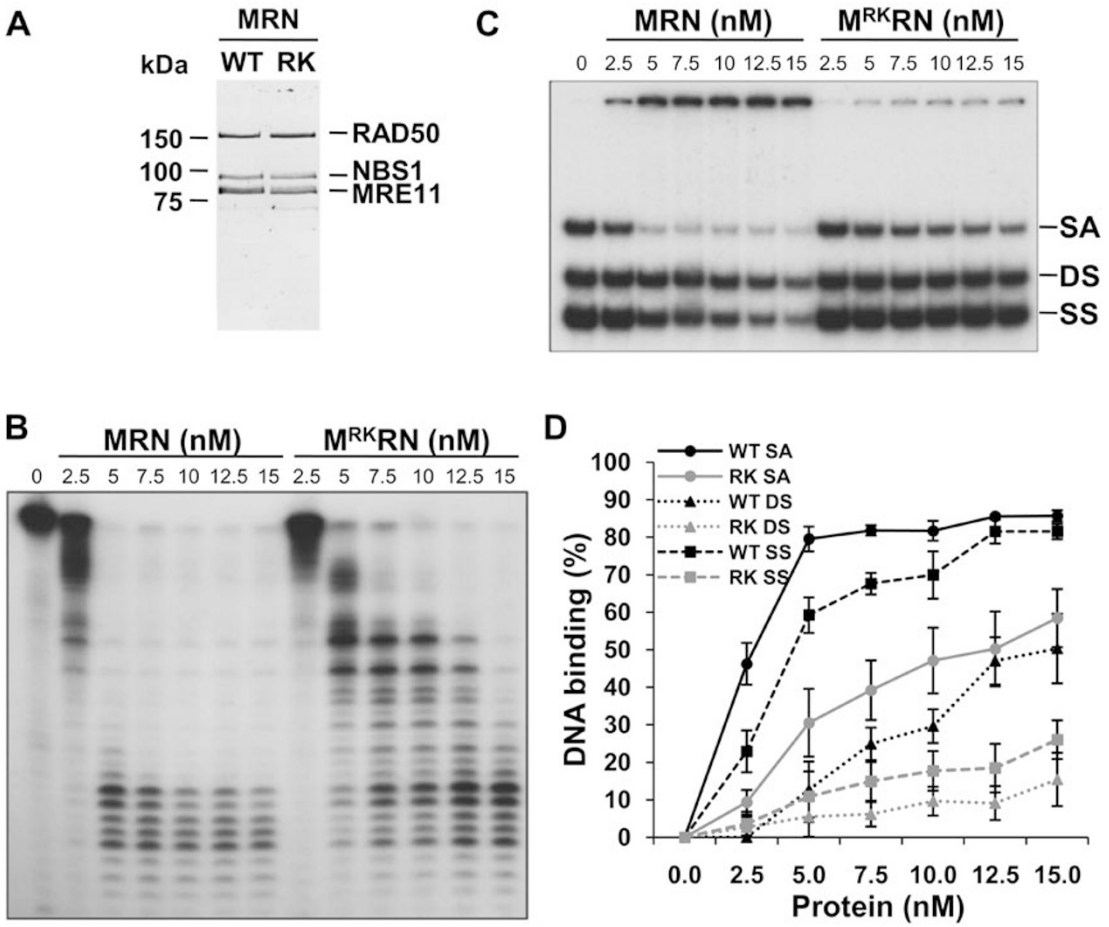

Figure 7 Defect in exonuclease activity and DNA binding of $M^{RK}RN$ complex. **(A)** SDS-PAGE of purified wild-type MRN (WT) and $M^{RK}RN$ (RK). **(B)** Exonuclease assays of MRN (2.5-15 nM) and $M^{RK}RN$ (2.5-15 nM) on dsDNA. The concentration of protein is calculated in function of MRE11. **(C)** Competition electrophoretic mobility shift assays were performed with MRN or $M^{RK}RN$ and ssDNA (SS), dsDNA (DS) and splayed arm (SA) substrates. The concentration of protein is calculated in function of MRE11. **(D)** Quantification of the DNA binding of panel **C**.

in *Mre11*$^{RK/RK}$ MEFs. We observed that increasing the protein levels of wild-type MRE11 in the *Mre11*$^{RK/RK}$ MEFs rescued the CHK1 phosphorylation defect (Figure 6D, lanes 9 and 10), but increasing the protein levels of MRE11^{RK} had little or no effect on CHK1 activation (Figure 6D, lanes 11 and 12). The MRE11^{RK} protein level in the MRE11^{RK} viral vector-infected *Mre11*$^{RK/RK}$ MEFs was comparable to that in the empty viral vector-infected wild-type MEFs (see MRE11 panel, Figure 6D, comparing lanes 11 and 12 with lanes 1 and 2). These findings show that *Mre11*$^{RK/RK}$ MEFs with restored MRE11^{RK} to levels of endogenous wild-type MRE11 still display impaired ATR/CHK1 activation. These findings show that the lack of a functional MRE11 GAR motif directly contributes to the ATR/CHK1 activation defects observed in *Mre11*$^{RK/RK}$ MEFs.

Defective exonuclease activity and DNA binding of M^{RK}RN complex

The presence of RPA-coated single-strand DNA (RPA-ssDNA) promotes ATR-ATRIP recruitment, which leads to CHK1 phosphorylation and activates the G_2/M checkpoint [44]. Hence, the CHK1 activation defect in *Mre11*$^{RK/RK}$ MEFs might result from abnormal DNA resection, leading to a reduction in RPA-ssDNA formation. To assess these molecular mechanisms, we first monitored whether purified $M^{RK}RN$ displayed DNA resection defects compared to the wild-type MRN complex (Figure 7A). We showed previously that recombinant MRE11^{RK} had impaired 3′-5′ exonuclease activity *in vitro* [36, 37], and we now extend these findings to show that MRE11^{RK} within the $M^{RK}RN$ complex also has impaired 3′-5′ exonuclease activity. Interestingly, three times more $M^{RK}RN$

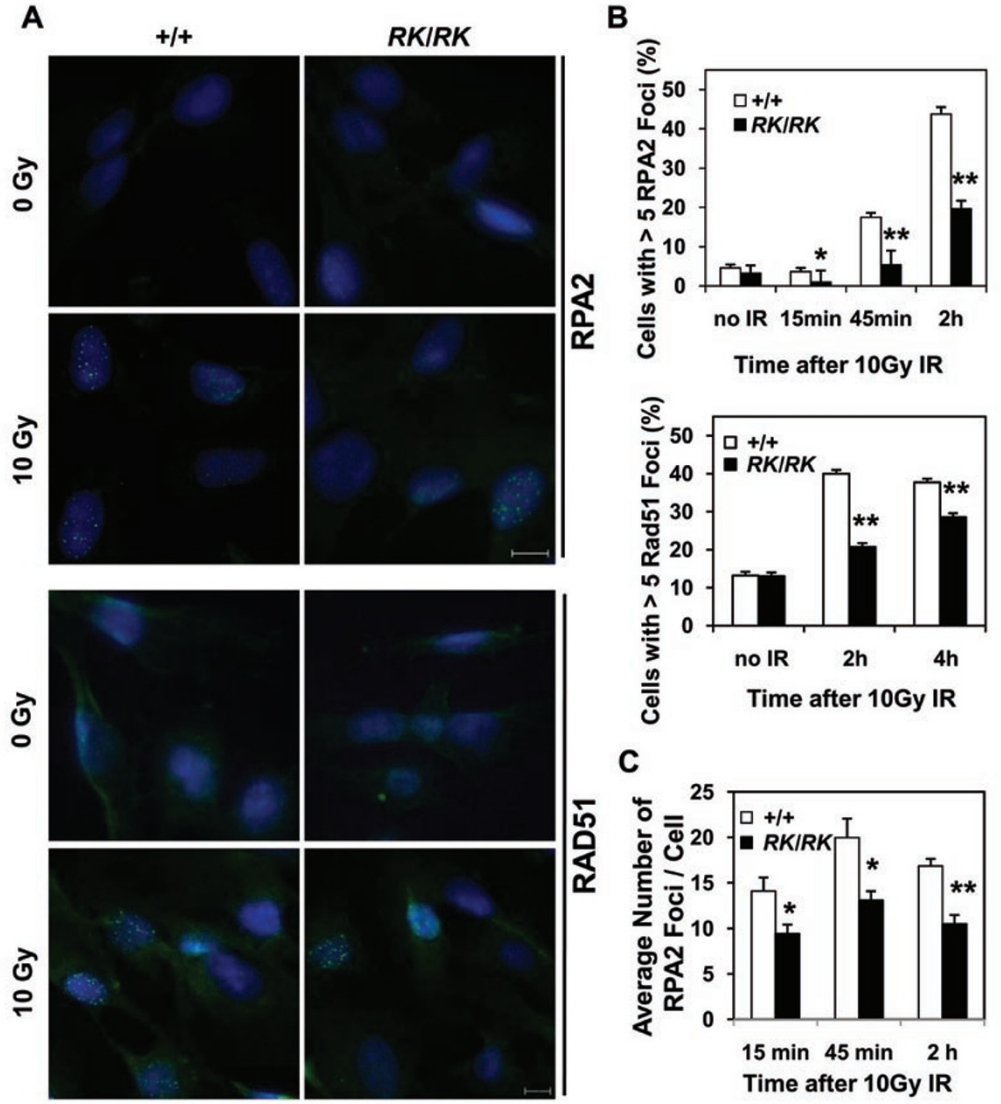

Figure 8 *Mre11*$^{RK/RK}$ MEFs have defects in IR-induced RPA2 and RAD51 foci formation. *Mre11*$^{+/+}$ and *Mre11*$^{RK/RK}$ MEFs, respectively, were left untreated or treated with 10 Gy of IR. After varying hours of recovery, the cells were visualized by indirect immunofluorescence with anti-RPA2 or anti-RAD51 antibody. **(A)** A typical image was shown for each sample. **(B)** The cells with > 5 foci were counted and expressed as a percentage. The graph shows the average and standard error of the mean (SEM) from two independent experiments performed in duplicates, where > 20 different fields were analyzed. In total, more than 500 cells were counted for each sample in each experiment. Statistical significance was assessed using Student's *t*-test. **P* < 0.05 and ***P* < 0.001. **(C)** The number of foci in the cells with > 5 RPA2 foci was counted. The graph shows the average number of foci in each cell, which has > 5 RPA2 foci and SEM from two independent experiments performed in duplicates. In total, more than 40 cells were counted for each sample. Statistical significance was assessed using Student's *t*-test. **P* < 0.01 and ***P* < 0.001.

was required to achieve the same level of DNA resection as MRN, suggesting that the M^{RK}RN complex has impaired resecting activity (Figure 7B, compare MRN at 5 nM and M^{RK}RN at 15 nM). In addition, we performed a DNA-binding analysis comparing the ability of the MRN and M^{RK}RN complexes to bind ssDNA, dsDNA and splayed arm DNA. As expected, the MRN complex bound both dsDNA and ssDNA, as well as splayed arm DNA (Figure 7C, 7D). The M^{RK}RN complex bound all three types of DNA with relative weaker affinity than the MRN complex (Figure 7C, 7D). For example, at the concentration of 5 nM, the wild-type MRN complex bound almost 80% splayed arm DNA, whereas the M^{RK}RN complex bound only 30% splayed arm DNA (Figure 7D).

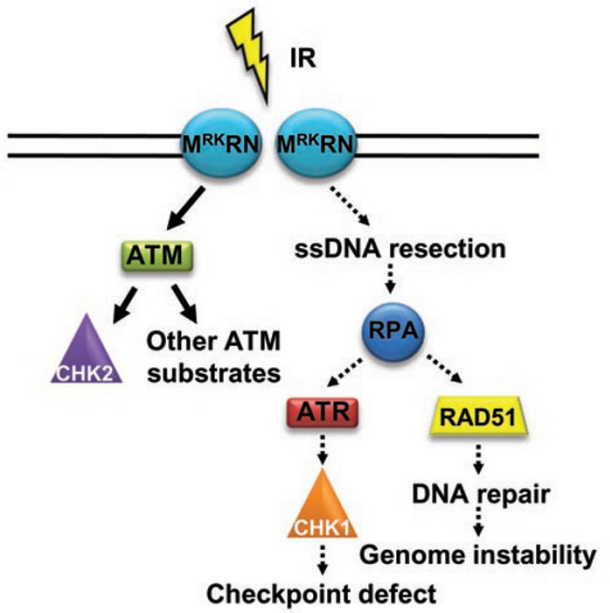

Figure 9 Model. The MRE11 GAR motif is required for IR-induced ssDNA resection and ATR activation but not for ATM activation. Defects in the MRE11 GAR motif lead to defects in RPA-ssDNA complexes, leading to defects in ATR and CHK1 activation. Subsequently, RAD51 cannot be properly recruited, leading to DNA repair defects and genomic instability.

These findings suggest that the DNA-binding ability of MRE11 may be required for the processivity of its intrinsic exonuclease activity.

Defective IR-induced RPA2 and RAD51 foci formation in Mre11$^{RK/RK}$ MEFs

To assess whether RPA-ssDNA complexes were formed in *Mre11*$^{RK/RK}$ MEFs, we assayed RPA foci formation in response to DSBs using anti-RPA2 antibodies after IR treatment. We observed a more than 50% decrease of *Mre11*$^{RK/RK}$ MEFs containing >5 RPA2 foci compared to wild-type MEFs (Figure 8A, 8B). Since RPA-ssDNA complexes are subsequently replaced with RAD51 for homologous recombination to proceed [45, 46], we examined the formation of RAD51 foci. Indeed, we also observed a significant reduction in RAD51 foci formation in *Mre11*$^{RK/RK}$ MEFs (Figure 8A, 8B). Two hours after 10 Gy IR treatment, ~40% of wild-type MEFs had > 5 RAD51 foci compared to ~20% in *Mre11*$^{RK/RK}$ MEFs (Figure 8A, 8B). At 4 h, ~40% of the wild-type MEFs retained > 5 RAD51 foci, while the *Mre11*$^{RK/RK}$ MEFs with >5 RAD51 foci increased to nearly 30%. Moreover, *Mre11*$^{RK/RK}$ MEFs had less RPA2 foci per cell than wild-type MEFs (Figure 8C). These results show that the *Mre11*$^{RK/RK}$ MEFs are defective in recruiting RPA and RAD51 to DSBs.

Discussion

In the present study, we have generated a mouse knock-in allele of *Mre11* that substitutes the arginines with lysines in the GAR motif. The *Mre11*$^{RK/RK}$ mice were sensitive to γ-IR and the MEFs isolated from the *Mre11*$^{RK/RK}$ mice accumulated increased number of aberrant chromosomes, defining a physiological role for the GAR motif in maintaining genomic stability. The *Mre11*$^{RK/RK}$ MEFs displayed defects of ATR/CHK1 signaling and G_2/M checkpoint activation, and reduced recruitment of RPA and RAD51 proteins to the damaged sites in response to γ-IR. MRE11^{RK} was assembled normally within the M^{RK}RN complex, localized to sites of DNA damage and normally activated the ATM pathway. *In vitro* biochemical analysis suggested that the M^{RK}RN complex exhibited defects in exonuclease processivity and DNA binding, which are likely to be responsible for the impaired DNA end resection and ATR/CHK1 activation observed in the *Mre11*$^{RK/RK}$ MEFs in response to IR. Our findings provide genetic evidence for the critical role of the MRE11 GAR motif in DSB repair, and define a mechanistic link between the MRE11 GAR motif, MRN exonuclease processivity, the processing of DSBs and cell cycle checkpoint activation (Figure 9).

The GAR motif is a characteristic signature of clusters of methylated arginines. The arginines located within the GAR motif have been shown to mediate protein-protein and protein-nucleic acid interactions [2]. Moreover, the GAR motif was shown to regulate protein localization, but this may be indirect due to protein-protein and protein-nucleic acid interactions. Using the unique genetic system and several biochemical and cytological methods, we demonstrate the molecular mechanism by which GAR motif regulates MRE11 function for the activation of ATR signaling and recruitment of RPA and RAD51 proteins to the DNA damage sites, both of which rely on ssDNA resection, a relatively later event of MRE11 action in response to DSBs. In contrast, the GAR motif mutation did not affect the initial response of the MRN complex to DSBs, as it was normally recruited to sites of DNA damage and normally activated the ATM pathway. The *Mre11*$^{RK/RK}$ mice provide an important tool to study the roles of the MRN complex at the later stage in response to DNA damage.

The physiological function of the MRE11 nuclease domain was assessed by the generation of mice carrying the nuclease-defective *Mre11*^{H129N} mutation [30]. Homozygous *Mre11*$^{H129N/H129N}$ mice are embryonically lethal,

Table 2 Comparison of *Mre11*$^{RK/RK}$ with *Mre11*$^{ATLD1/ATLD1}$ and *Mre11*$^{H129/H129}$ mice and MEF cells

	MRE11$^{RK/RK}$	MRE11$^{ATLD1/ATLD1}$	MRE11$^{H129/H129}$
Mouse embryonic development	Normal	Normal	Lethal
Fertility	Normal	Reduced	—
Sensitivity to IR (MEF cells)	Yes	Yes	Yes
IR-induced G2/M checkpoint	Defect	Defect	Normal
IR-induced ATM and CHK2 phosphorylation	Normal	Defect	Normal
IR-induced CHK1 phosphorylation	Defect	NA	NA

like *Mre11*-null mice, confirming the requirement for the MRE11 nuclease domain during embryogenesis. Cells from *Mre11*$^{H129N/H129N}$ mice exhibited hypersensitivity to IR and genomic instability. The M^{H129N}RN complex was stable, localized to sites of DNA damage and activated ATM. The cellular defect of *Mre11*$^{H129N/H129N}$ mice lies in their inability to properly repair DNA by homologous recombination [30]. We demonstrated significant impairment of the 3′-5′ exonuclease processivity of the M^{RK}RN complex (Figure 7) [36, 37]. The intrinsic activity of nuclease activities of MRE11 may be sufficient to promote fork degradation [47]. In conjunction with other factors, such as 5′-3′ exonucleases CtIP and EXO1, the MRN complex is functionally involved in the extensive degradation, leading to DNA end resection and homologous recombination [15, 16, 48, 49]. Our findings suggest that the GAR motif may modulate the MRE11 exonuclease activity within the MRN complex *in vivo*, contributing to the defective ssDNA resection observed in *Mre11*$^{RK/RK}$ MEFs (Figure 8).

The impaired DNA-binding activity of MRE11^{RK} that we observed may also contribute to the defect of DNA end processing observed with the M^{RK}RN complex. The MRE11 GAR motif is likely to be required to bind selective types of DNA ends at the sites of DNA damage to modulate ATR activation during DSB repair. Indeed, we found that MRN bound splayed arm DNA, representative of a DNA replication intermediate, preferentially over ssDNA and dsDNA substrates. We infer that the MRE11 exonuclease activity is required to generate ssDNAs needed to activate the ATR pathway via ssDNA binding by ATRIP. The fact that *Mre11*$^{RK/RK}$ mice are viable, suggests that the exonuclease defect we that observed is not as severe as observed in *Mre11*$^{H129N/H129N}$ mice in which both exonuclease and endonuclease activities are defective [30]. We observed that *Mre11*$^{RK/RK}$ MEFs display a G_2/M checkpoint defect not observed in *Mre11*$^{H129N/H129N}$ MEFs [30]. These findings suggest that some phenotypes of *Mre11*$^{RK/RK}$ MEFs cannot be solely explained by impaired MRE11 exonuclease activity (Table 2). As such, it is important to note that cells from ATR-deficient Seckel Syndrome [50], like *Mre11*$^{RK/RK}$ MEFs, also display a G_2/M checkpoint defect. In addition, we observed the formation of radial chromosomes in *Mre11*$^{RK/RK}$ MEFs (Figure 3A and Table 1), a feature also observed in ATR and Fanconi-deficient cells. Our results suggest that defects in the methylation of mammalian MRE11 GAR motif are likely to manifest themselves as defects in the level of ATR activation, leading to genomic instability and cell death.

In conclusion, our findings provide genetic and biochemical evidence for the critical role of the MRE11 GAR motif in DSB repair. Our data define a mechanistic link between the MRE11 GAR motif, MRN exonuclease processivity, DSB end processing and cell cycle checkpoint activation. The fact that the GAR motif is widely found in proteins implies that this mechanism of regulation may also occur in other systems.

Materials and Methods

Reagents and antibodies

Rabbit anti-MRE11 antibodies were from Novus Biologicals (Littleton, CO, USA), Cell Signalling Technology (Danvers, MA, USA) and GeneTex Inc. (Irvine, CA, USA), respectively. Rabbit anti-53BP1, anti-RAD50 and anti-mouse NBS1 antibodies were from Novus Biologicals. Mouse anti-ATM-pS1981 (mouse Ser1987) antibody was from Rockland (Gilbertsville, PA, USA). Mouse anti-γH2AX monoclonal antibody, rabbit anti-phosphohistone H3-Ser10, ASYM25b, and anti-CHK2 antibodies were obtained from Millipore (Billerica, MA, USA). Rabbit anti-RAD51, anti-CHK1 and anti-CDC25A antibodies were from Santa Cruz Biotechnology (Santa Cruz, CA, USA). Rabbit anti-phospho-CHK1 ser345 antibody was from Cell Signalling Technology. Rabbit anti-acetyl-lysine antibody was from Abcam (Cambridge, MA, USA). Rabbit anti-RPA2 antibodies were generated with a peptide located at the C-terminal end of the mouse RPA2 using the following peptide as antigen, NEGHIYSTVDDDHFKSTDAEC. Propidium iodide (PI) and the Alexa Fluor 488-conjugated goat anti-rabbit antibodies and anti-mouse antibodies were from Invitrogen (Carlsbad, CA, USA). Protein A-sepharose and mouse anti-α-tubulin monoclonal antibody were from Sigma (St Louis, MO, USA). Protease inhibitor cocktail and protein phosphatase inhibitor cocktail were from Roche (Mississauga, ON, USA). CHK1 substrate peptide (KKKVSRSGLYRSPENLNRPR) derived from

CDC25C was purchased from AnaSpec Inc. (San Jose, CA, USA). Immunoprecipitations and immunoblotting were performed as previously described [5].

Generation of the Mre11$^{RK/RK}$ mice

The mutant *Mre11* knock-in allele (*Mre11^{RK}*) was generated using a targeting construct 3lox-2frt flanking a neomycin resistance cassette for selection [5]. The primers used to introduce arginine to lysine mutations were: 5′-CTGCCCTTTGGCTCCTTTCTTC-CCTTTGCCTTTGCCTTTGCCTTTGCTCGGCACTGCTG-3′ and 5′-AATTCGGCACCTAAAGGAGGCTCTCAGAAAGGC-CGAGGTCAGCACC-3′. For the 5′ arm of the construct, a 3.2 kb DNA fragment was amplified using the following oligonucleotides: 5′-TTTTCCGCGGATGGAATCTGAACACACACT-GAGTGG-3′ and 5′-TTTTGCGGCCGCATGTTTGTAAAAGA-CAGTCATGAG-3′ and the fragment was subcloned into *Sac*I and *Not*I unique sites of the pGK-neo vector. A 3.1 kb fragment for the 3′ arm was amplified by PCR with 5′-TTTTGTCGAC-TACTATCAGGAGATAAAGTACTTACATG-3′ and 5′-TTTTG-GCCGGCCTGAAAGATGTAGTCCTGTCAC-3′ and subcloned into *Sal*I and *Fse*I. To insert the mutated exon 14 of *Mre11*, gDNA was amplified and engineered to have *Asc*I and *Xho*I ends. The completed vector was then sequenced to verify the absence of any undesired mutations. In order to clearly identify the mutated allele, an *Eco*RI site was introduced, also changing serine at position 583 to an asparagine. An *Fse*I site was introduced at the 3′ end of the 3.1 kb fragment and was used to linearize the plasmid for electroporation into embryonic stem (ES) cells. Potential homologous recombinant ES cells emerging from neomycin selection were screened, as determined through a long template PCR system (Roche, 11681842001). Primers for verification included: 5′ arm: ATTGGCACCTATTGTGCAGC and AGGTCGAGGGAC-CTAATAACTTCG, 3′ arm: GCGTGCAGAATGCCGGGCTTC-CGGAG and GATCTGAAAGCTAGTATG, and the fragment between the insert and 5′ arm: AGTGCAGTCAGTGCTCTTTA and CTCTCATTCAGTCATATCAA. Approximately 500 ES colonies were screened and several clones were identified that contained the *Mre11* mutant allele. Targeted ES cells were injected into 3.5-day-old blastocytes and were transferred into CD-1 foster mothers, and animals classified as chimeras by coat color were mated with C57BL/6 mice. Germline transmission was achieved and mice were maintained in C57BL/6 background. These mice were then crossed with a transgenic mouse containing FLP1 recombinase gene (Jackson Lab) under the direction of the Gt(ROSA)26Sor promoter to promote recombination and removal of the neomycin cassette. The resulting DNA sequence yielded an ~600 bp band in the recombinant allele due to the insertion of 90 bp encompassing the loxP and FRT site of the vector.

Mouse genotyping and RT-PCR of the Mre11 transcript

All mouse procedures were performed in accordance with McGill University guidelines, which are set by the Canadian Council on Animal Care. Genomic DNA was isolated from ear biopsies and analyzed by PCR analysis. The *Mre11* allele was identified using the following oligonucleotides: 5′-TGTAGTAGAACT-TGGACAGT-3′ and 5′-TGAACCCAGGTCATCTAGAA-3′ yielding a 525 bp band in the wild-type allele and a 591 bp band in the *Mre11^{RK}* allele. Total cellular RNA was prepared by TRIzol reagent according to the manufacturer's protocol (Invitrogen) to ensure proper splicing of the knock-in transcript. Total RNA (6 μg) was reverse transcribed, and cDNA samples were subjected to PCR analysis. The following 5′ and 3′ primers were used to evaluate the *Mre11* transcript: 5′-GCGGTTTCTTAAGGAGCGCCATATT-3′ and 5′-TGTGCCCGACCACCTTTGATCAGCC-3′, yielding a 550 bp band.

Isolation, immortalization and culture of MEFs

Primary MEFs were isolated from E14.5 embryos. Spontaneously immortalized MEFs were created according to the standard 3T3 protocol. All cells were grown in DMEM containing 10% fetal bovine serum.

Ionizing radiation treatment of mice and MEFs

Mice and cells were irradiated at room temperature using a Theratron T-780 Cobalt Unit located in the Department of Radiation Oncology at the Jewish General Hospital (Montreal, Quebec, Canada). Doses ranging from 2 to 10 Gy were delivered at a dose rate of 0.66 Gy/min. The cells were returned to an incubator after the IRs and maintained at 37 °C for further analysis. For *in vivo* survival experiments, 8- to 10-week-old mice (n = 7) of each genotype were whole-body irradiated at a dose of 10 Gy and then monitored for radiation toxicity.

Chromosome breakage studies: scoring of chromosome aberrations

We have analyzed more than 50 Giemsa-stained metaphases for the passage 7 MEFs without and passage 2 MEFs with 1 Gy IR for each genotype, respectively. The number and type of structural chromosome abnormalities were scored. Chromatid and isochromatid gaps, chromatid and isochromatid breaks, deletions and fragments were scored as a single break. Structural rearrangements including translocations and radial figures were scored as two breakage events. The total number of chromosome aberrations and the mean number of chromosome aberrations per metaphase were scored. Diploid and tetraploid cells were analyzed separately.

Clonogenic assay

Approximately 200-400 cells were plated on 10 cm dishes and treated with varying dosage of IR in duplicate 24 h after plating. The cells were maintained in the regular medium and allowed to grow for 14-20 days. The colonies were fixed and stained with 0.1% crystal violet for 30 min. The stained colonies were counted. The surviving fraction was determined by dividing the average number of colonies for each treatment by the average number of colonies in the control plates.

Class switch recombination

Breeding and genotyping of mice harboring combinations of the *Mre11^{cond}*, *Mre11$^{\Delta}$*, *Mre11^{H129N}* and *CD21-Cre* alleles were as previously described [23, 30]. Analyses of CSR was as previously described [23].

Cytometry analysis

For all flow cytometry experiments, both cells growing on the surface of the dishes and in the culture medium were harvested, fixed with 75% ethanol and stored at −20 °C for less than 1 week before staining and analysis. All flow cytometry measurements were performed using BD FACSCalibur flow cytometer (BD Bio-

sciences). Data were analyzed using BD CellQuest Pro software. For measurement of phosphorylated histone H3, fixed cells were first stained with anti-H3 pS10 rabbit antibody for 1 h and then with FITC-conjugated goat anti-rabbit IgG (Invitrogen) for another hour after washing with dilution buffer (1% FBS and 0.1% Triton X-100 in PBS) as described previously [5]. Cells were then counterstained with PI and subjected to flow cytometry analysis.

Immunofluorescence

Cells growing on glass coverslips were washed with PBS twice and fixed with 4% paraformaldehyde at room temperature for 10 min. The cells were then permeabilized (0.5% Triton X-100 in PBS) for 10-15 min. Following three washes with PBS, cells were blocked with 10% serum in PBS and stained with mouse anti-γH2AX (1:1 000), anti-MRE11 (1:200), rabbit anti-53BP1 (1:200), anti-RPA2 (1:100) or anti-RAD51 (1:20) antibodies diluted in PBS containing 5% serum and 0.1% Triton X-100. After three washes, the cells were then stained with Alexa Fluor 488-conjugated goat anti-rabbit or anti-mouse secondary antibodies. DNA was counterstained with 4,6-diamidino-2-phenylindole after three washes with PBS and coverslips were mounted with Immu-Mount purchased from Thermo Scientific. Images were taken using a Zeiss M1 fluorescence microscope.

CHK1 activity assays

MEFs were lysed with lysis buffer (10 mM Tris-HCl, pH 7.4, 150 mM NaCl supplemented with phosphatase inhibitor cocktails and protease inhibitor cocktails) and whole-cell lysates were incubated with anti-CHK1 antibody for 2 h and then protein A-sepharose beads for 1 h. The beads were then washed three times with lysis buffer and then twice with kinase reaction buffer (50 mM Tris-HCl, pH 7.0, 1 mM DTT, 5 mM $MgCl_2$, 0.4 mM $MnCl_2$). The washed beads were resuspended in 20 µl kinase reaction buffer containing 10 µg peptide and 10 µCi γ-^{32}P-ATP and incubated at 30 °C for 20 min with rotation. After spinning for 10 s at 4 °C, the reaction tubes were placed on ice and immediately 10 µl of supernatant was spotted onto thick Fisherbrand Whatmann paper. The papers were then washed five times with 0.5% orthophosphoric acid and rinsed once with ethanol and dried. After drying, the papers were counted with a multi-purpose Scintillation Counter LS 6500, Beckman Coulter (Mississauga, ON, USA). The CHK1 activity was expressed as percentage of the activity in the non-treated samples.

Purification of MRN and M^{RK}RN

MRN and M^{RK}RN were purified as follows. Insect cells (800 ml, 10^6 cells/ml) were co-infected with MRE11-HIS (or MRE11^{RK}-HIS) and FLAG-RAD50 dual baculovirus and a GST-NBS1 baculovirus for 48 h in a spinner flask. The cells were collected by centrifugation and the pellet was frozen on dry ice. Cells were lysed in PBS300 (1× PBS, 150 mM NaCl, 1 mM EDTA, 1 mM DTT, 0.05% Triton X-100, and protease inhibitors). The cell lysate was centrifuged in 35 000 rpm. for 40 min. Glutathione Sepharose (2 ml, GE Healthcare) was added to the supernatant and incubated for 1.5 h at 4 °C. The beads were washed three times with PBS300, twice with PBS500 (1× PBS, 350 mM NaCl, 1 mM EDTA, 1 mM DTT, 0.05% Triton X-100 and protease inhibitors) and once with P5 buffer (20 mM $NaPO_4$, pH 7.0, 500 mM NaCl, 10% glycerol, 0.02% Triton X-100, 5 mM imidazole). The MRN complex was eluted by cleavage with PreScission protease (60 U/ml, GE Healthcare) for 5 h at 4 °C. The supernatant was added to 400 µl of Talon resin (Clontech) and incubated for 1.5 h at 4 °C. The resin was washed with 10 ml of P30 Talon washing buffer (20 mM $NaHPO_4$, pH 7.4, 1 M NaCl, 10% glycerol, 0.02 % Triton X-100, 30 mM imidazole). MRN complexes were eluted with buffer containing 500 mM imidazole and dialyzed in storage buffer (20 mM Tris-Cl, pH 7.5, 200 mM NaCl, 10% glycerol, 1 mM DTT).

Exonuclease and DNA-binding assays

Exonuclease assays were performed as described previously [36]. DNA-binding reactions (10 µl) contained ^{32}P-labelled DNA oligonucleotides (25 nM in nucleotides of each substrate) and MRN or M^{RK}RN, at the indicated concentrations, in binding buffer (25 mM MOPS (morpholinepropanesulfonic acid), pH 7.0, 60 mM KCl, 0.2% Tween, 2 mM DTT, 1 mM $Mg(CH_3COO)_2$). Reaction mixtures were incubated at 37 °C for 15 min, followed by 15 min of fixation in 0.2% glutaraldehyde. Reactions were loaded on an 8% TBE acrylamide gel.

Acknowledgments

We thank Mélanie Morel for expert technical assistance. We thank Drs Eric Brown, John Petrini and Junjie Chen for helpful discussions and Dr David Cortez for reagents. We also thank Julie Birraux for MRN baculoviruses and Cyril Charbonnel for technical help. This study was supported by grant MOP-67070 from the Canadian Institutes of Health Research to SR. JH is supported by a grant from the Cancer Research Network of Fonds de la Recherche en Santé du Québec. DOF is supported by NIH R01 HL079118 and the Leukemia and Lymphoma Society. JYM is a FRSQ Chercheur Senior supported by funds from the CIHR (MOP-102722). SR is a Chercheur-National of the Fonds de la recherche en Santé du Québec.

References

1 Bedford MT, Richard S. Arginine methylation an emerging regulator of protein function. *Mol Cell* 2005; **18**:263-272.
2 Bedford MT, Clarke SG. Protein arginine methylation in mammals: who, what, and why. *Mol Cell* 2009; **33**:1-13.
3 Tang J, Kao PN, Herschman HR. Protein-arginine methyltransferase I, the predominant protein-arginine methyltransferase in cells, interacts with and is regulated by interleukin enhancer-binding factor 3. *J Biol Chem* 2000; **275**:19866-19876.
4 Pawlak MR, Scherer CA, Chen J, Roshon MJ, Ruley HE. Arginine N-methyltransferase 1 is required for early postimplantation mouse development, but cells deficient in the enzyme are viable. *Mol Cell Biol* 2000; **20**:4859-4869.
5 Yu Z, Chen T, Hébert J, Li E, Richard S. A mouse PRMT1 null allele defines an essential role for arginine methylation in genome maintenance and cell proliferation. *Mol Cell Biol* 2009; **29**:2982-2996.
6 Boisvert FM, Chénard CA, Richard S. Protein interfaces in signaling regulated by arginine methylation. *Sci STKE* 2005; **271**:re2.
7 Mirzoeva OK, Petrini JH. DNA damage-dependent nuclear dynamics of the Mre11 complex. *Mol Cell Biol* 2001; **21**:281-

288.
8 Lisby M, Barlow JH, Burgess RC, Rothstein R. Choreography of the DNA damage response: spatiotemporal relationships among checkpoint and repair proteins. *Cell* 2004; **118**:699-713.
9 Berkovich E, Monnat RJJ, Kastan MB. Roles of ATM and NBS1 in chromatin structure modulation and DNA double-strand break repair. *Nat Cell Biol* 2007; **9**:683-690.
10 Hopfner KP, Craig L, Moncalian G, *et al.* The Rad50 zinc-hook is a structure joining Mre11 complexes in DNA recombination and repair. *Nature* 2002; **418**:562-566.
11 Williams RS, Moncalian G, Williams JS, *et al.* Mre11 dimers coordinate DNA end bridging and nuclease processing in double-strand-break repair. *Cell* 2008; **135**:97-109.
12 Lee JH, Paull TT. Direct activation of the ATM protein kinase by the Mre11/Rad50/Nbs1 complex. *Science* 2004; **304**:93-96.
13 Falck J, Coates J, Jackson SP. Conserved modes of recruitment of ATM, ATR and DNA-PKcs to sites of DNA damage. *Nature* 2005; **434**:605-611.
14 Jazayeri A, Falck J, Lukas C, *et al.* ATM- and cell cycle-dependent regulation of ATR in response to DNA double-strand breaks. *Nat Cell Biol* 2006; **8**:37-45.
15 Sartori AA, Lukas C, Coates J, *et al.* Human CtIP promotes DNA end resection. *Nature* 2007; **450**:509-514.
16 Limbo O, Chahwan C, Yamada Y, *et al.* Ctp1 is a cell-cycle-regulated protein that functions with Mre11 complex to control double-strand break repair by homologous recombination. *Mol Cell* 2007; **28**:134-146.
17 Mimitou EP, Symington LS. Sae2, Exo1 and Sgs1 collaborate in DNA double-strand break processing. *Nature* 2008; **455**:770-774.
18 Zhu Z, Chung WH, Shim EY, Lee SE, Ira G. Sgs1 helicase and two nucleases Dna2 and Exo1 resect DNA double-strand break ends. *Cell* 2008; **134**:981-994.
19 Mirzoeva OK, Petrini JH. DNA replication-dependent nuclear dynamics of the Mre11 complex. *Mol Cancer Res* 2003; **1**:207-218.
20 Williams RS, Williams JS, Tainer JA. Mre11-Rad50-Nbs1 is a keystone complex connecting DNA repair machinery, double-strand break signaling, and the chromatin template. *Cell Biol* 2007; **85**:509-520.
21 Xie A, Kwok A, Scully R. Role of mammalian Mre11 in classical and alternative nonhomologous end joining. *Nat Struct Mol Biol* 2009; **16**:814-818.
22 Rass E, Grabarz A, Plo I, *et al.* Role of Mre11 in chromosomal nonhomologous end joining in mammalian cells. *Nat Struct Mol Biol* 2009; **16**:819-824.
23 Dinkelmann M, Spehalski E, Stoneham T, *et al.* Multiple functions of MRN in end-joining pathways during isotype class switching. *Nat Struct Mol Biol* 2009; **16**:808-813.
24 Deng Y, Guo X, Ferguson DO, Chang S. Multiple roles of MRE11 at uncapped telomeres. *Nature* 2009; **460**:914-918.
25 Stewart GS, Maser RS, Stankovic T, *et al.* The DNA double-strand break repair gene hMRE11 is mutated in individuals with an ataxia-telangiectasia-like disorder. *Cell* 1999; **99**:577-587.
26 Carney JP, Maser RS, Olivares H, *et al.* The hMre11/hRad50 protein complex and Nijmegen breakage syndrome: linkage of double-strand break repair to the cellular DNA damage response. *Cell* 1998; **93**:477-486.
27 Shiloh Y. ATM and related protein kinases: safeguarding genome integrity. *Nat Rev Cancer* 2003; **3**:155-168.
28 Luo G, Yao MS, Bender CF, *et al.* Disruption of mRad50 causes embryonic stem cell lethality, abnormal embryonic development, and sensitivity to ionizing radiation. *Proc Natl Acad Sci USA* 1999; **96**:7376-7381.
29 Xiao Y, Weaver DT. Conditional gene targeted deletion by Cre recombinase demonstrates the requirement for the doublstrand break repair Mre11 protein in murine ES cells. *Nucl Acid Res* 1997; **15**:2985-2991.
30 Buis J, Wu Y, Deng Y, *et al.* Mre11 nuclease activity has essential roles in DNA repair and genomic stability distinct from ATM activation. *Cell* 2008; **135**:85-96.
31 Zhu J, Petersen S, Tessarollo L, Nussenzweig A. Targeted disruption of the Nijmegen breakage syndrome gene NBS1 leads to early embryonic lethality in mice. *Curr Biol* 2001; **11**:105-109.
32 Theunissen JW, Kaplan MI, Hunt PA, *et al.* Checkpoint failure and chromosomal instability without lymphomagenesis in Mre11(ATLD1/ATLD1) mice. *Mol Cell 2003*; **12**:1511-1523.
33 Difilippantonio S, Celeste A, Fernandez-Capetillo O, *et al.* Role of Nbs1 in the activation of the Atm kinase revealed in humanized mouse models. *Nat Cell Biol* 2005; **7**:675-685.
34 Paull TT, Gellert M. The 3′-5′ exonuclease activity of Mre 11 facilitates repair of DNA double-strand breaks. *Mol Cell* 1998; **1**:969-979.
35 de Jager M, Dronkert ML, Modesti M, *et al.* DNA-binding and strand-annealing activities of human Mre11: implications for its roles in DNA double-strand break repair pathways. *Nucleic Acids Res* 2001; **29**:1317-1325.
36 Déry U, Coulombe Y, Rodrigue A, *et al.* A glycine-arginine domain in control of the human MRE11 DNA repair protein. Mol Cell Biol 2008; **28**:3058-3069.
37 Boisvert FM, Déry U, Masson JY, Richard S. Arginine methylation of MRE11 by PRMT1 is required for DNA damage checkpoint control. *Genes Dev* 2005; **19**:671-676.
38 Kraus M, Alimzhanov MB, Rajewsky N, Rajewsky K. Survival of resting mature B lymphocytes depends on BCR signaling via the Igalpha/beta heterodimer. *Cell* 2004; **117**:787-800.
39 Zhou BB, Elledge SJ. The DNA damage response: putting checkpoints in perspective. *Nature* 2000; **408**:433-439.
40 Bakkenist CJ, Kaston MB. DNA damage activates ATM through intermolecular autophosphorylation and dimer dissociation. *Nature* 2003; **421**:499-506.
41 Brown EJ, Baltimore D. Essential and dispensable roles of ATR in cell cycle arrest and genome maintenance. *Genes Dev* 2003; **17**:615-628.
42 Myers JS, Cortez D. Rapid activation of ATR by ionizing radiation requires ATM and Mre11. *J Biol Chem* 2006; **281**:9346-9350.
43 Mailand N, Falck J, Lukas C, *et al.* Rapid destruction of human Cdc25A in response to DNA damage. *Science* 2000; **288**:1425-1429.
44 Zou L, Elledge SJ. Sensing DNA damage through ATRIP recognition of RPA-ssDNA complexes. *Science* 2003; **300**:1542-1548.
45 Sugiyama T, Zaitseva EM, Kowalczykowski SC. A single-

stranded DNA-binding protein is needed for efficient presynaptic complex formation by the *Saccharomyces cerevisiae* Rad51 protein. *J Biol Chem* 1997; **272**:7940-7945.

46 Benson FE, Stasiak A, West SC. Purification and characterization of the human Rad51 protein, an analogue of *E. coli* RecA. *EMBO J* 1994; **13**:5764-5771.

47 Schlacher K, Christ N, Siaud N, *et al.* Double-strand break repair-independent role for BRCA2 in blocking stalled replication fork degradation by MRE11. *Cell* 2011; **145**:529-542.

48 Uanschou C, Siwiec T, Pedrosa-Harand A, *et al.* A novel plant gene essential for meiosis is related to the human CtIP and the yeast COM1/SAE2 gene. *EMBO J* 2007; **26**:5061-5070.

49 Mimitou EP, Symington LS. DNA end resection: many nucleases make light work. *DNA Repair* 2009; **8**:983-995.

50 Andreassen PR, D'Andrea AD, Taniguchi T. ATR couples FANCD2 monoubiquitination to the DNA-damage response. *Genes Dev* 2004; **18**:1958-1963.

(**Supplementary information** is linked to the online version of the paper on the *Cell Research* website.)